Earth and Planetary Science Letters 453 (2016) 78–86

Contents lists available at ScienceDirect

Earth and Planetary Science Letters

www.elsevier.com/locate/epsl

Persistent high paleosecular variation activity in southern hemisphere for at least 10 000 years

Catherine Constable [a,*], Monika Korte [b], Sanja Panovska [a]

[a] Cecil H. and Ida M. Green Institute of Geophysics and Planetary Physics, Scripps Institution of Oceanography, University of California at San Diego, 9500 Gilman Drive, La Jolla, CA 92093-0225, USA
[b] Helmholtz-Zentrum Potsdam Deutsches GeoForschungsZentrum – GFZ Telegrafenberg, D-14473 Potsdam, Germany

ARTICLE INFO

Article history:
Received 30 November 2015
Received in revised form 4 August 2016
Accepted 8 August 2016
Available online 24 August 2016
Editor: B. Buffett

Keywords:
geomagnetism
paleomagnetism
paleomagnetic field models
South Atlantic Magnetic Anomaly

ABSTRACT

Direct observations of the geomagnetic field show that secular variation is strong in the Atlantic hemisphere, and comparatively reduced in the Pacific region. The dipole has been decaying since at least 1840 AD, driven by growth and migration of reverse flux patches in the southern hemisphere. We investigate whether anything like this modern pattern of geomagnetic secular variation persists and can be detected in global paleomagnetic field models. Synthesis of results from two new time-varying spherical harmonic models shows that geographically distinct geomagnetic secular variation extends to at least 10 000 BP. The models use the same database but differ in methodology, leading to some regional differences in results. Consistent large-scale surface features include strong average fields in the northern hemisphere and weaker fields with greater overall variability in the south. Longitudinal structure is present, with weaker average fields in the western Pacific than in the east, and prominent negative inclination anomalies extending beneath Indonesia, across Africa and to Brazil, but weaker anomalies in the central Pacific. Marginally positive inclination anomalies occur west of the Americas. Paleosecular variation activity peaks at high southern latitudes, and there is a pattern of reduced activity at equatorial and mid-latitudes beneath the Pacific. Although the dipole has exhibited both growth and decay over the interval 0–10 000 BP, our results show that geomagnetic paleosecular variation is preferentially focused in similar geographic regions to secular variation seen in the modern field.

1. Introduction

Geomagnetic secular variation since 1600 AD has revealed a dynamic and still evolving region of low field strength in the South Atlantic (Jackson et al., 2000). In contrast to the active Atlantic hemisphere, recent geomagnetic secular variation beneath the Pacific region appears relatively placid as can be seen in Fig. 1 which shows the average structure of the radial magnetic field at the core mantle boundary for 1590–1990 AD and a measure of its temporal variability in the form of the standard deviation about the mean value. This geographical focus of secular variation activity has been confirmed and sharpened using recent satellite observations from the Oersted, CHAMP, and SAC-C missions (Holme et al., 2011; Finlay et al., 2012), and the origin of recent dipole decay has been associated with the growth of reverse flux patches (Gubbins et al., 2006). The poleward migration of reverse flux patches on the core–mantle boundary (CMB) has been suggested as a possible mechanism for geomagnetic reversals (Gubbins, 1987), and some (Hulot et al., 2002; Olson, 2002; Olson et al., 2009; De Santis and Qamili, 2015) have suggested the South Atlantic Anomaly may be a precursory signature of an incipient geomagnetic reversal. Others have interpreted the decay in the longer term context of paleofield observations (Constable and Korte, 2006; Olson and Amit, 2006; Wang et al., 2015; Laj and Kissel, 2015), and note that the current field decrease is compatible with a return to values more like the average value over the past few million years. The recent rapid dipole decrease is too fast to be solely attributed to free Ohmic decay (Olson and Amit, 2006) and has been hypothesized to result from flux expulsion (Gubbins, 1987) or equator-ward transport of high latitude magnetic flux (Olson and Amit, 2006).

Detailed studies of field morphology in time varying geomagnetic field models covering the past 10 and 400 yrs reveal the general motion of magnetic features at the CMB (Finlay et al., 2012), and core surface flow models (Gillet et al., 2009) which are derived from such models indicate a gyre-like structure circulating northward on the eastern side of the Indian Ocean, westwards towards Africa and South America, before migrating south again. It

* Corresponding author.
E-mail address: cconstable@ucsd.edu (C. Constable).

http://dx.doi.org/10.1016/j.epsl.2016.08.015

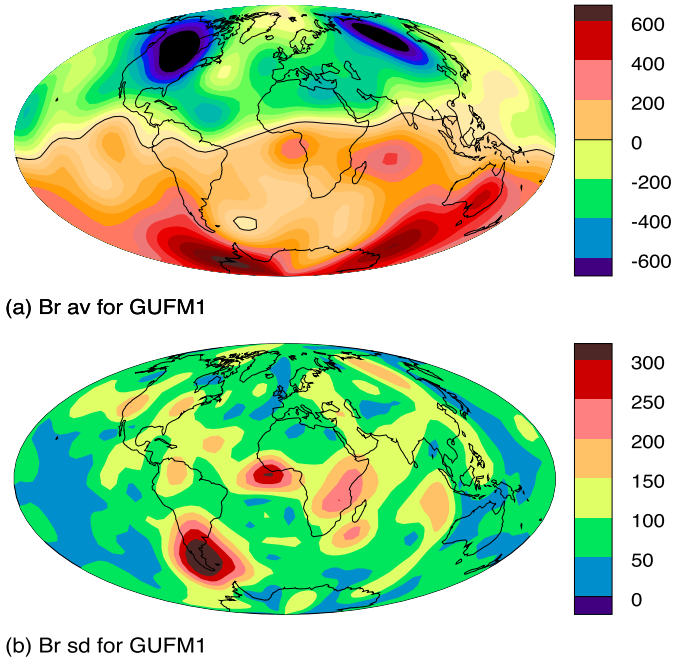

Fig. 1. (a) Average B_r (in μT) at CMB and (b) its standard deviation over the time interval 1590–1990 AD for model *gufm1*. Note the high variability from westward drift of low latitude flux patches in the Atlantic hemisphere, and beneath Southern America.

is obviously of great interest to determine whether this is a stable long-term pattern of field behavior or simply a temporary feature coincident with the current period of direct observations. If the former then it provides interesting support for the popular idea (Willis et al., 2007; Aubert et al., 2013) that the dynamics of the geomagnetic field can be strongly influenced by laterally varying structure in its boundary conditions.

Understanding of the geodynamo has flourished with the advent of numerical simulations capable of reproducing Earth-like properties such as dominantly dipolar fields, geomagnetic reversals, and excursions. Considerable effort has been focused on understanding the consequences of variable boundary conditions derived from seismic structure in the lowermost mantle, and compatible with the current field (Olson, 2002; Aubert et al., 2007; Davies et al., 2008; Driscoll, 2015). Geographic structure in secular variation may be linked both to inner core structure (Aubert et al., 2013) and to thermal and compositional heterogeneity manifest as large low seismic velocity provinces in the D" region just above the core–mantle boundary (Lekic et al., 2012; Ziegler and Constable, 2015). New interpretations of paleomagnetic observations can help determine the relative importance of top and bottom boundary conditions invoked in many numerical dynamos.

However, an accurate view of the longer term geomagnetic field structure has proved elusive because of the lack of definitive time-varying paleomagnetic field models. These require globally distributed data, reliable uncertainty estimates, and a clear understanding of the limitations of the modeling strategies to uncover any departures of average fields from the most basic geocentric axial dipole model and reveal any regions where the secular variation is consistently more active than elsewhere.

Over the past two decades considerable progress has been made in building time-varying global paleomagnetic field models (Constable and Korte, 2015). Strategies used for modern field modeling have been adapted to the paleofield, and systematic efforts have been directed to providing uniform community access to all available data through archiving in online databases like Geomagia.v3 (http://geomagia.gfz-potsdam.de) and MagIC (http://earthref.org/MAGIC/, Tauxe et al., 2016). Selected data sets used in specific field models can be found at EarthRef.org's ERDA archive (https://earthref.org/ERDA/). A recent study by Panovska et al. (2015) compared various strategies for inversion and determined that the resulting models were quite sensitive to the assignment of data uncertainties and initial data calibration which needs to be based on the best absolute information available. That work identified deficiencies in some existing paleofield models, but stopped short of producing any definitive model for the 0 to 10 ka interval. Here we draw on that experience to present two new models, and a synthesis of the results. For the latter we rely on identifying characteristic statistical properties of the models since a direct geodynamical interpretation is not possible given the distribution and quality of the data. The properties include geographic variations in Holocene temporal averages and standard deviations of various parameters that can be predicted from the models.

2. Data, models, and the paleosecular variation activity index

Globally distributed paleomagnetic data from archeological artifacts and young volcanics combined with those from lacustrine and marine sediments are the basis for our new time-varying regularized geomagnetic field models that span the past 10 000 yrs. Archeomagnetic and volcanic data preserve a record of the field in the form of thermal remanent magnetization. We used data available from the GEOMAGIA50.v3 database (Brown et al., 2015), comprising 5083 inclination, 3610 declination and 4145 intensity data in the time interval 8000 BC to 1990 AD. The sediment data (67365 in total), which provide broader global coverage and carry a record of post-depositional remanent magnetization, are the same collection as used in the recent investigation of modeling methods (Panovska et al., 2015) mentioned above. The individual sediment records and their references are listed in the supplementary material for that article and the digital data are available online at EarthRef.org in the ERDA archive at https://earthref.org/ERDA/2101/. Our archeomagnetic data set differs slightly from that used by Panovska et al. (2015) because of corrections and updates to GEOMAGIA50.v3 (Brown et al., 2015) up to April 30, 2015. The archeomagnetic dataset as used here is available from ERDA at https://earthref.org/ERDA/2206.

An overview of average departures observed from the signal expected from a geocentric axial dipole is given in Fig. 2, a figure showing inclination anomalies (relative to an axial dipole field) and paleointensity as a function of latitude for the entire data set used to construct our new models. There is considerable scatter in these observations arising from several sources: (1) merging data spanning 0–10 ka, over which time there has been considerable secular variation in the geomagnetic field; (2) longitudinal variations in spatial geomagnetic field structure; (3) inherent uncertainty in the paleomagnetic record. In Fig. 2(a) the blue dotted line provides a smoothing spline fit to the inclination anomaly data, revealing marginally positive average anomalies between about 10 and 40°S and significant negative anomalies in the northern hemisphere. The spline fit for intensity data in Fig. 2(b) shows that north of 40°S the observations indicate systematically higher field strength than from an axial dipole contribution alone.

Several new data sets have been published in the course of our work, and one of particular significance comes from the Southern hemisphere where data distributions are generally sparser than in the North. Lake Mavora records from New Zealand (Turner et al., 2015) were not included in our modeling as they were not yet available at that time. However, we have added them to Fig. 2, where it can be seen they exhibit the same basic signal as other data used in our models. The Mavora results are compatible with our overall conclusions. That said, the New Zealand data will provide valuable input to future models because they are a significant

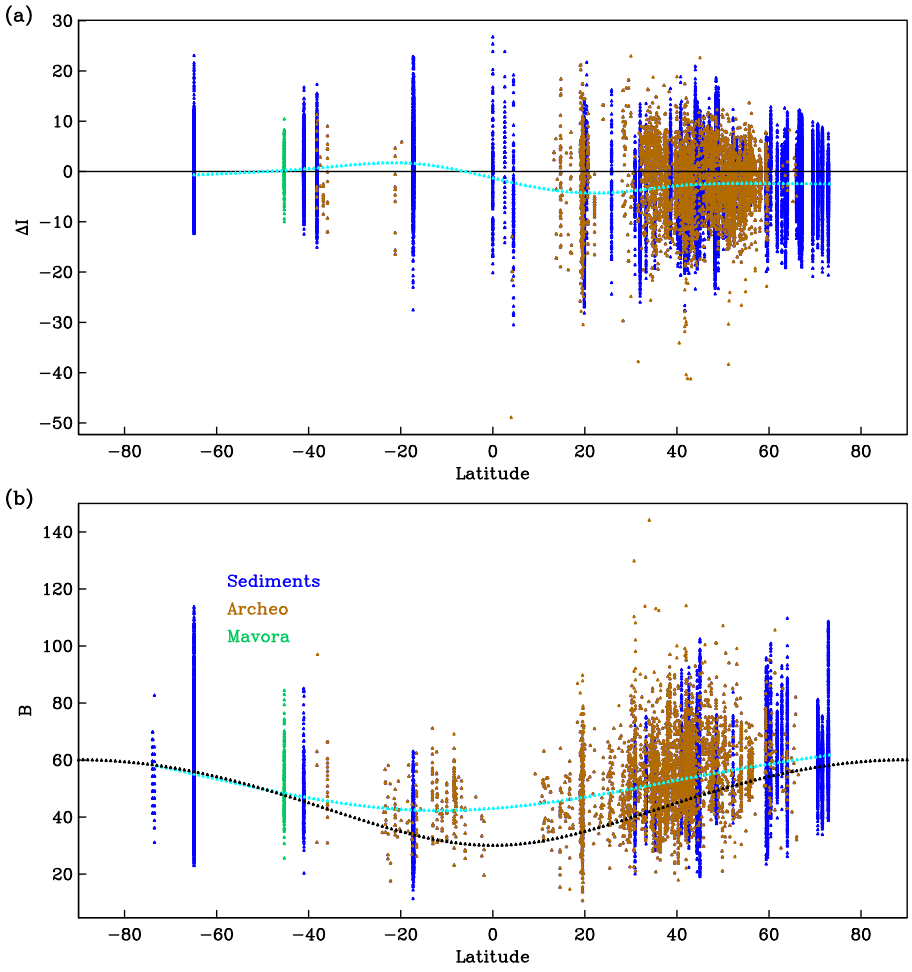

Fig. 2. Latitudinal variation in (a) the paleomagnetic inclination anomaly (in degrees) relative to that expected for an axial dipole field, and (b) paleointensity (in μT) for data used to construct *CALS10k.2* and *HFM.OL1.A1*. Blue symbols represent sediment and brown archeomagnetic or volcanic sources. Initial calibration of the sediment paleointensity comes from *ARCH10k.1*. Green symbols are data from Lake Mavora (Turner et al., 2015), not included in our new models. Blue dotted lines in (a) and (b) are smoothing spline fits to the observations. Black dotted line gives the latitudinal variation in intensity expected from the average axial dipole term in *CALS10k.2*. Note the systematic deviations from the axial dipole signal in both inclination anomaly and field intensity. (For interpretation of the references to color in this figure, the reader is referred to the web version of this article.)

addition to the Southern Hemisphere collection and their chronology does reveal significant differences from earlier records.

2.1. Models

Three new models were constructed for this study, termed *ARCH10k.1*, *CALS10k.2* and *HFM.OL1.A1*. Details about the modeling methods can be found in Panovska et al. (2015). As for previous models in the *CALS* and *HFM* series all the new ones have spatial representations in spherical harmonics to degree and order 10, while time variations are parameterized in cubic B-splines with knots positioned every 40 yrs. The models are regularized via a penalty function trading normalized L1 or L2 data misfits against minimization of quadratic model norms (in this case the Ohmic dissipation norm (Gubbins, 1975) and the 2nd time derivative of the magnetic field) severely limiting their spatial resolution above about degree 4 and temporal resolution at periods less than a few hundred years.

ARCH10k.1 is based on absolute archeomagnetic and volcanic data and serves solely as a tool in the construction of the two new models. It provides initial calibration for relative declination and intensity records from sediments and is not intended for use as an adequate representation of the global field for the past 10 ky. As can be seen in Fig. 2 the archeomagnetic and volcanic data set (brown symbols) is spatially biased towards the northern hemisphere. It is also dominated by the most recent 3 ky in age, inevitably leading to a model that is predominantly dipolar during its early epochs and generally lacking in structure in the southern hemisphere throughout the whole time interval. The modelling method is the same as for *CALS10k.2* except that (in the absence of sediment data) no calibration of intensity or re-orientation of declination is required. Fig. 3 shows predictions of Virtual Axial Dipole Moment (VADM) and inclination anomaly relative to an axial dipole field from the 10 ky temporal average of *ARCH10k.1* and Fig. 7(a), (d) provides the same perspective for B_r at the CMB as was given in Fig. 1 for *gufm1*.

CALS10k.2 and *HFM.OL1.A1* are dominated by sediment records extending to 10 ky. The same initial data set and uncertainty estimates for individual sediment records are used in each case. The uncertainties are based on the cross-validation approach to local spline fitting and comparisons with archeomagnetic data (Panovska et al., 2012). These time series provide only relative variations in paleointensity and often no absolute orientation for declination, and must be calibrated using the best available absolute information. Primary calibration of relative paleointensity (RPI) observations and relative declinations is an important issue, and the results are sensitive to the model used for calibration. The two new models differ from one another in the iterative methods used to derive absolute calibrations and orientations, although each uses predictions from *ARCH10k.1* for the first calibration.

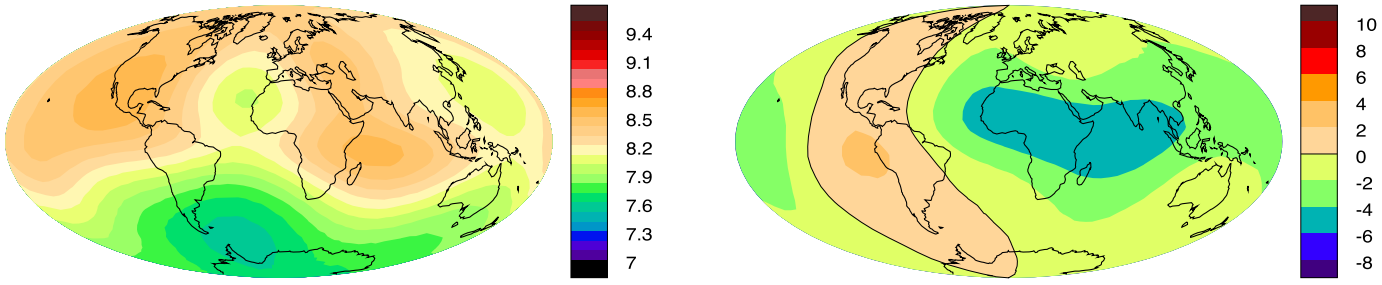

Fig. 3. (a) VADM (in units of 10^{22} A m^2) and (b) inclination anomaly (in degrees) for precursory model *ARCH10k.1* used to supply initial intensity calibrations for *CALS10k.2* and *HFM.OL1.A1*, and as a starting model for *HFM.OL1.A1*.

Table 1
Some parameters for the precursory and final 0–10 ka models.

Model	Data A, V	Data Sed	Rejected (%)	RMS	Ψ (nT^2)	Φ (nT^{2}a^{-4})
ARCH10k.1	12838	0	2.6	1.68	10.9×10^{12}	4.22
CALS10k.2	12838	67365	3.9	1.09	13.3×10^{12}	5.81
HFM.OL1.A1	12838	67365	0.6	1.09	11.0×10^{12}	27.81

Data A, V and Sed are the initial number of data, available for time interval 8000 BC to 1990 AD, for archeological plus volcanics materials and for sediments, respectively. RMS is the root mean square misfit normalized by the uncertainty estimates. Ψ and Φ are the spatial and temporal norms, respectively. These values are for time intervals 8000 BC to 1600 AD. Note that *CALS10k.2* is constrained to agree with *gufm1* from 1600–1990 AD, but *HFM.OL1.A1* simply makes use of any available paleodata.

For *CALS10k.2* a geocentric axial dipole with $g_1^0 = 30$ μT is used as the starting model in the inversion of the calibrated data. The L2 measure of misfit between model and data is used along with iterative outlier rejection at the level of three standard deviations resulting in a smaller final dataset. The recent part of the model is constrained to agree with *gufm1* taking due account of the lack of intensity control prior to 1840 AD.

For *HFM.OL1.A1*, *ARCH10k.1* is used as the starting model in the non-linear iterative inversion. It invokes the L1 measure of misfit between model and data and rejects data with residuals larger than five standard deviations. The L1 misfit is implemented by iteratively reweighted least squares (Constable, 1988), retaining more data than in *CALS10k.2*, but putting lower weight on data that cannot be fit well. Co-estimation of RPI calibration and declination orientation values during the inversion in some cases leads to slightly different final calibration and re-orientation values from *CALS10k.2*. There is no requirement for *HFM.OL1.A1* to agree with *gufm1*: it only uses paleomagnetic observations.

Table 1 lists the numbers of data, rms misfit, spatial and temporal norms for each model. As can be seen from the model norms, *CALS10k.2* model is slightly smoother in time (but not in spatial variations) than *HFM.OL1.A1*, reflecting differences in choice of the relevant damping parameters. This is also evident in the time series of dipole moment variations and in the spatial power spectra (see Fig. 4).

2.2. Paleosecular variation activity index

The average radial field at the CMB (see Fig. 1) provides one means of detecting geographic structure in the time-averaged field and its standard deviation over some time interval serves as a proxy for the level of secular variation. The PSV index (Panovska and Constable, 2016) provides an alternative measure of field complexity at Earth's surface, that can be evaluated locally for a specific time $P_i(\theta, \phi, t)$, or as a local temporal average $\bar{P}_i(\theta, \phi)$, and its standard deviation over time, $\sigma_{P_i}(\theta, \phi)$, is a measure of PSV activity. Here t is time and θ, ϕ are geographic colatitude and longitude, respectively. For a field model like *gufm1*, maps of $P_i(\theta, \phi, t)$ and $\bar{P}_i(\theta, \phi)$ serve as proxies for instantaneous and average deviation (in both direction and strength) from a "normal" stable geocentric axial dipole field. Local field strength in the form of a virtual dipole moment (VDM) is defined relative to the "normal" current full dipole moment $M_0 = 80$ ZA m^2. As has often been the case in paleosecular variation studies (Merrill et al., 1996), directional departures from a geocentric axial dipole are quantified by angular deviation of the virtual geomagnetic pole (VGP) from the geographic axis.

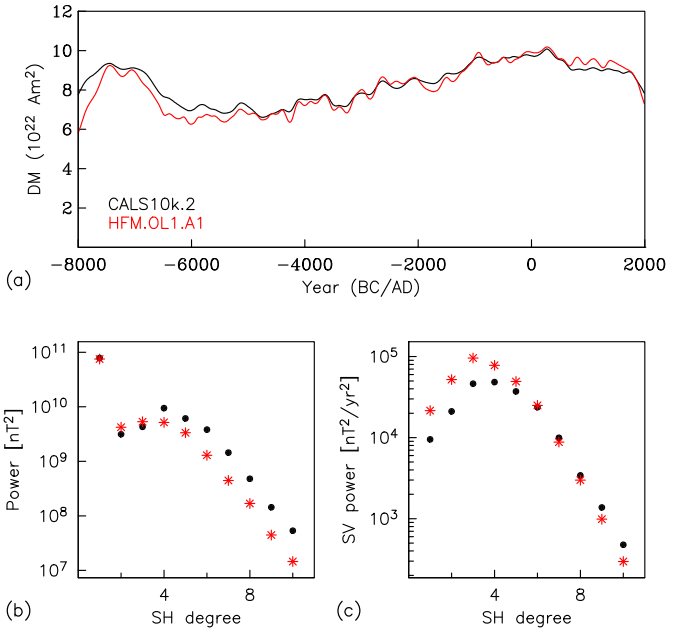

Fig. 4. Dipole moment variations with time and time-averaged spatial power spectra for the field and its secular variation for models *CALS10k.2* and *HFM.OL1.A1*. Note the differences in balance between temporal and spatial variability, with stronger secular variation but lower spatial complexity in *HFM.OL1.A1*.

$P_i(\theta, \phi, t)$ is a composite parameter incorporating both the paleomagnetic directions and field strength variations. It effectively uses VGP co-latitude (θ_p/π) as a local measure of deviation from an axial dipole field. This is actually expressed (Panovska and Constable, 2016) in terms of absolute value of the VGP latitude, λ_p, to allow for continuity when the VGP crosses the equator during an excursion or reversal. Taking the ratio of this term to the local virtual dipole moment, M normalized by the present day value $M_0 = 80$ ZA m^2 (M/M_0) we have

$$P_i(\theta, \phi, t) = \frac{[\pi/2 - |\lambda_p(\theta, \phi, t)|]/\pi}{M(\theta, \phi, t)/M_0} = \frac{[\pi/2 - |\lambda_p(\theta, \phi, t)|]M_0}{\pi\ M(\theta, \phi, t)} \quad (1)$$

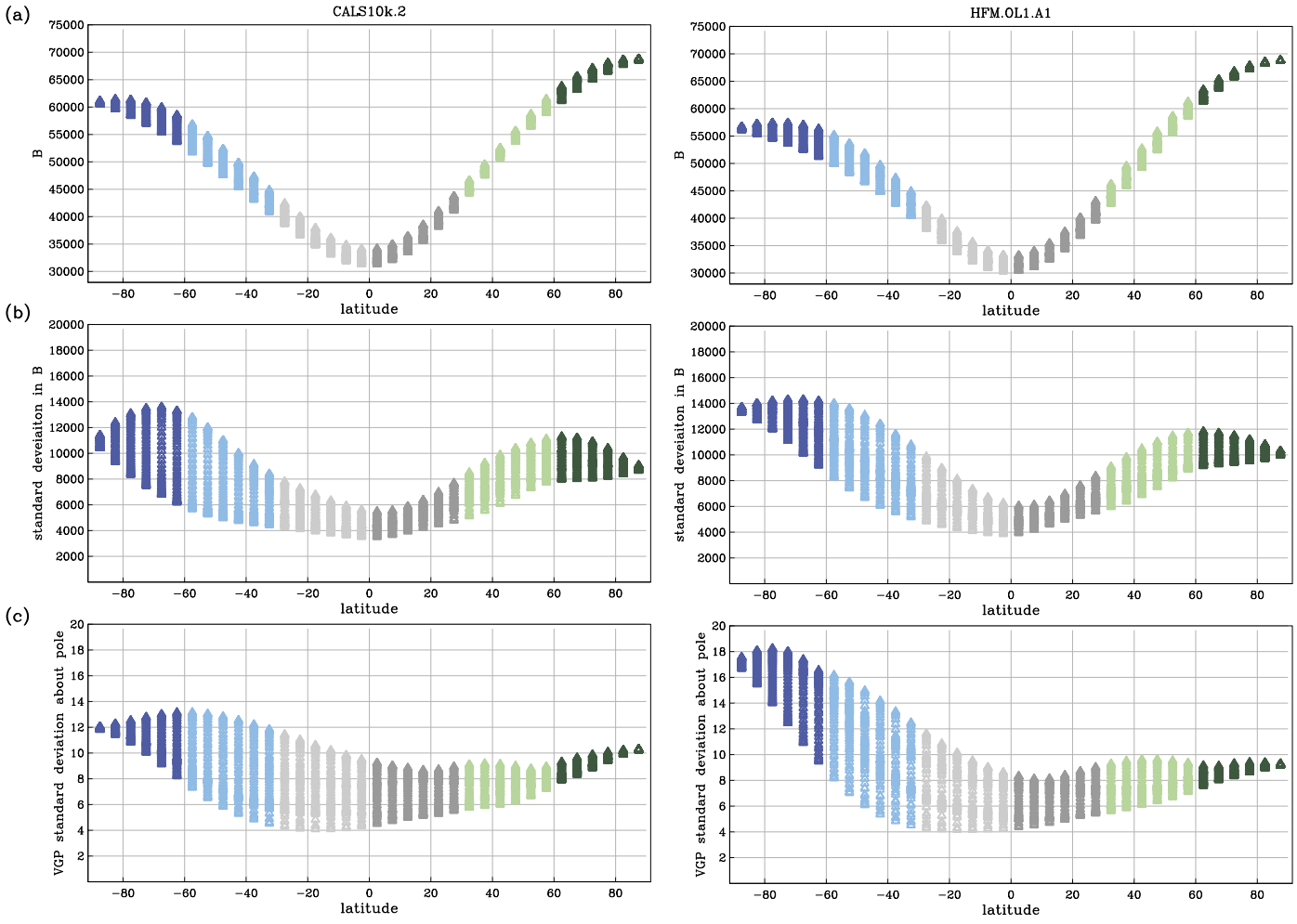

Fig. 5. Latitudinal variation in field properties at Earth's surface for models *CALS10k.2* and *HFM.OL1.A1*. At any given latitude each triangle represents a time average or temporal standard deviation for a specific location (the range of values are from samples equally spaced around a small circle in longitude). (a) Average field strength (in nT) over 10 ky interval spanned by the models; (b) Standard deviation in field strength (in nT) about the mean values given in (a); (c) VGP root mean square angular deviation (degrees) from the geographic pole arising from temporal field variations over 0–10 ka. Colors highlight latitude bands of width 30°. Note the contrast in amplitude and variability between equivalent latitudes in each hemisphere.

Note that both λ_p and M vary with location. When the VGP is located in the northern hemisphere $\theta_p(\theta,\phi,t) < \pi/2$ as expected for normal polarity stable fields we have $P_i = \frac{\theta_p\, M_0}{\pi\, M}$. Later we map $\bar{P}_i(\theta,\phi)$ time-averaged geographic variations in P_i for various models and also show the geographic temporal activity via $\sigma_{P_i}(\theta,\phi)$ the standard deviation about the mean value. This provides an rms measure for secular variability over the time span of the model.

3. Results

CALS10k.2 and *HFM.OL1.A1* supersede all previously presented models in both the *CALS* and *HFM* series (Korte and Constable, 2011; Korte et al., 2011; Panovska et al., 2015). The use of different modeling strategies on the same initial data set allows an assessment of robust features in the results, and the opportunity to identify important geodynamical processes. Predictions of local field strength, VADM, VGP dispersion, and inclination anomalies relative to the axial dipole are used to characterize the field at Earth's surface.

We begin with Fig. 5 which shows latitudinal variation in field properties at Earth's surface for models *CALS10k.2* and *HFM.OL1.A1*, and an overall departure from hemispheric symmetry about the equator. The average field strength in (a) is lower at southern latitudes than for equivalent northern latitudes, mainly reflecting the influence of an average axial quadrupole contribution of 4.7% or 6% of the dominant axial dipole term in *CALS10k.2* and *HFM.OL1.A1*, respectively. This is comparable to the time-averaged values of a few percent obtained for data sets spanning longer time intervals of a few million years (Johnson et al., 2008). The greater spread in average intensity values in the south reflects a stronger variation with longitude. Additionally, the greater variability in the southern hemisphere is reflected in the temporal standard deviations about the mean intensity values in Fig. 5(b) (compare light and dark blue regions in south with light and dark green in north), and in the VGP dispersions about the geographic pole in (c). Both temporal and spatial variability are explicitly suppressed by the regularization employed in the modeling process, so this is not an artifact arising from data distribution, but a requirement for adequate statistical fits to the data. At any given latitude in Fig. 5, the spread across the symbols shows the effect of longitudinal variability in the field model. This is most pronounced in the southern hemisphere. Again it is worth noting the greater overall temporal variability in *HFM.OL1.A1* (parts (b) and (c)), represented by the generally larger standard deviations than in *CALS10k.2*. While both models show similar structure in the results, the details differ slightly with the modeling strategies producing stronger overall

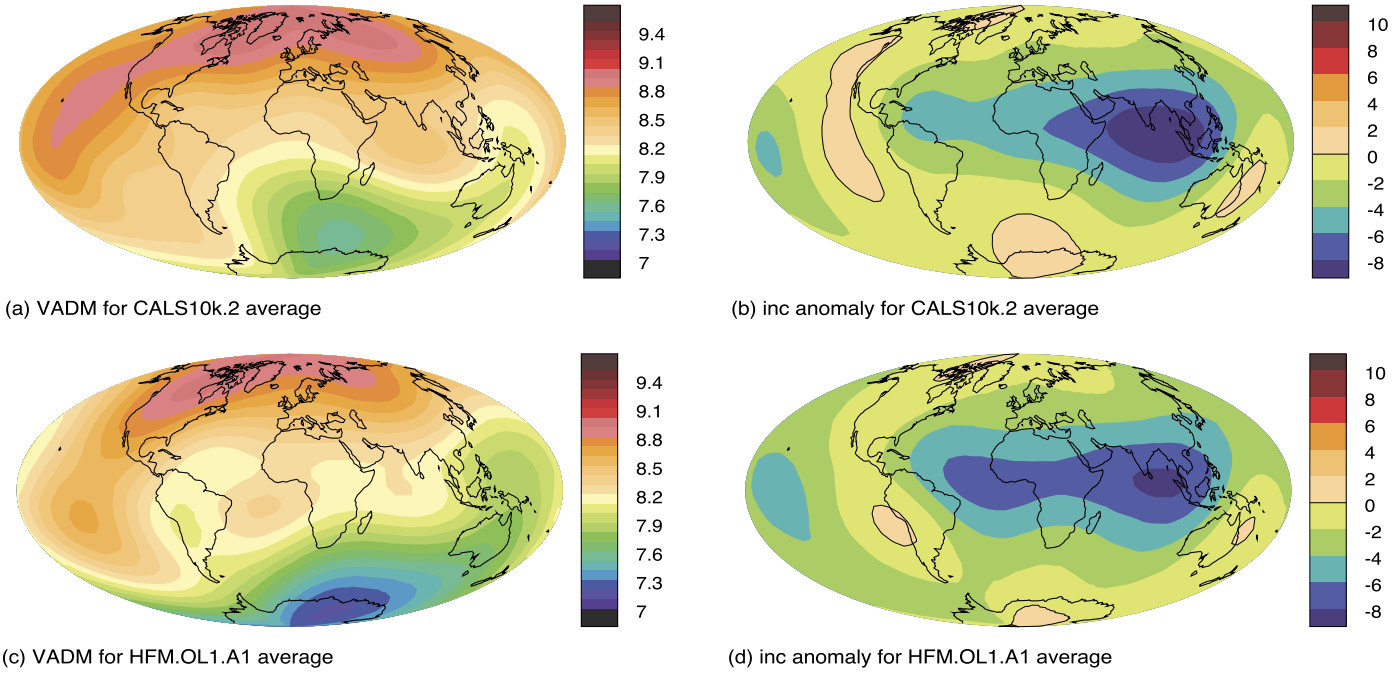

Fig. 6. VADM and inclination anomaly for models *CALS10k.2* and *HFM.OL1.A1* averaged over 0–10 ka. In (a), (c) the VADM (in units of 10^{22} A m^2) represents the moment of the equivalent geocentric axial dipole as a function of position. (b), (d) Give the inclination anomaly in degrees relative to that predicted by a geocentric axial dipole.

asymmetry in *HFM.OL1.A1*. The robustness of the main results in both models, despite differences in modeling procedures, ensure the reliability of our findings independent of data treatment or modelling methodology.

The longitudinal structure evident in the variability seen at each latitude in Fig. 5 is further exposed in Fig. 6, where gross geographic effects have been removed to show the temporally averaged geographic variation relative to that expected from a geocentric dipole aligned with the rotation axis. Here we see (in (a) and (c)) that the lowest average VADMs are concentrated at extreme southern latitudes and that below average values extend into the western equatorial Pacific. Peak negative inclination anomalies (parts (b) and (d)) relative to the purely latitudinal variation expected from the geocentric axial dipole fall near Indonesia, but extend in a broad equatorial swath as far as Brazil. Inclination anomalies in the Americas and west of there are small. This is also mainly the case above mid-latitudes and in the polar regions. The spatial structures in the two models are similar, but there are some differences in the anomaly amplitudes. For example, when averaged globally the VADM is 2.4% lower for *HFM.OL1.A1* (81.7 ZA m^2) than for *CALS10k.2* (83.7 ZA m^2). Similar figures for the preliminary calibration model, *ARCH10k.1* (Fig. 3) showed much less variability in the overall structure, a reflection of its overall inadequate data coverage in both time and space.

The 10 000 year averages represented in Fig. 6 are different in several ways from the structure of the modern field reconstructed in *gufm1* from direct observations made from 1590 to 1990 AD (Jackson et al., 2000), and in the higher resolution satellite dominated *gufm-sat* for the decade 2000 to 2010 (Finlay et al., 2012). The longer time interval produces a model with greatly reduced structure as mobile small scale variations are averaged out. The relative sparsity (especially in the southern hemisphere) and lower accuracy of paleomagnetic data cannot produce models of the same resolution as the modern field so that when downward continued to the core–mantle boundary under the assumption that the silicate mantle is well approximated by an insulator, the radial magnetic field lacks detail, especially in the form of the wave train of intense flux patches (Finlay et al., 2012) both north and south of the equator that underlie much of the westward drift seen at Earth's surface (compare Figs. 1(a) and 7(b), (c)). However, the large scale high latitude flux lobes surrounding the tangent cylinder are clearly present in *CALS10k.2*(b,e) and *HFM.OL1.A1* (c,f). It is worth noting that the average position of the northern hemisphere flux lobes differs from the 400 year average in *gufm1*. This confirms what has been seen already in numerous other models (Korte et al., 2009, 2011; Korte and Holme, 2010; Korte and Constable, 2011; Nilsson et al., 2014; Panovska et al., 2015). The detailed motions of the flux lobes have been tracked by (Amit et al., 2010) for the past 3 ky in the *CAL3k.3* model. There are also signs of unusual structure in the equatorial western Pacific, perhaps related to standing oscillatory structure observed in the historical field under Indonesia (Bloxham and Gubbins, 1985). The lack of structure in B_r and low temporal standard deviations in B_r at the CMB in Fig. 7(a, d) reflect again the paucity of southern hemisphere data in *ARCH10k.1*, and show that it should not be used as a measure of either average field or global secular variation for the Holocene. Fig. 7(e) and (f) do better, the spatial structures are broadly similar for *CALS10k.2* (b, e) and *HFM.OL1.A1*, with high levels of temporal variability most evident at latitudes coincident with the peak flux concentrations visible in B_r. It is worth noting however, that high variability does not appear restricted to the same longitudes as the average flux lobe positions. This is related to the eastward average location of the North American flux lobe compared with *gufm1*, probably reflecting the influence of some high values associated with high variability in B_r located approximately beneath Iceland.

The rapid field changes under the Indian Ocean that feature in modern satellite observations (Holme et al., 2011) have been proposed (Finlay et al., 2012, 2016) as part of a planetary scale gyre episodically transporting flux from high to low latitudes, and then westward under the Atlantic hemisphere. The detailed level of field changes and flow models available for more recent times cannot be recovered directly for the paleofield. However, the paleosecular variation index, P_i, and its standard deviation over time (see Section 2.2 and (Panovska and Constable, 2016)) serve as useful proxies for geographic variations in field structure and activity (Fig. 8). The largest values for the averaged 10 ky models are focused at high southern latitudes, and overall $\bar{P}_i$ is stronger in the

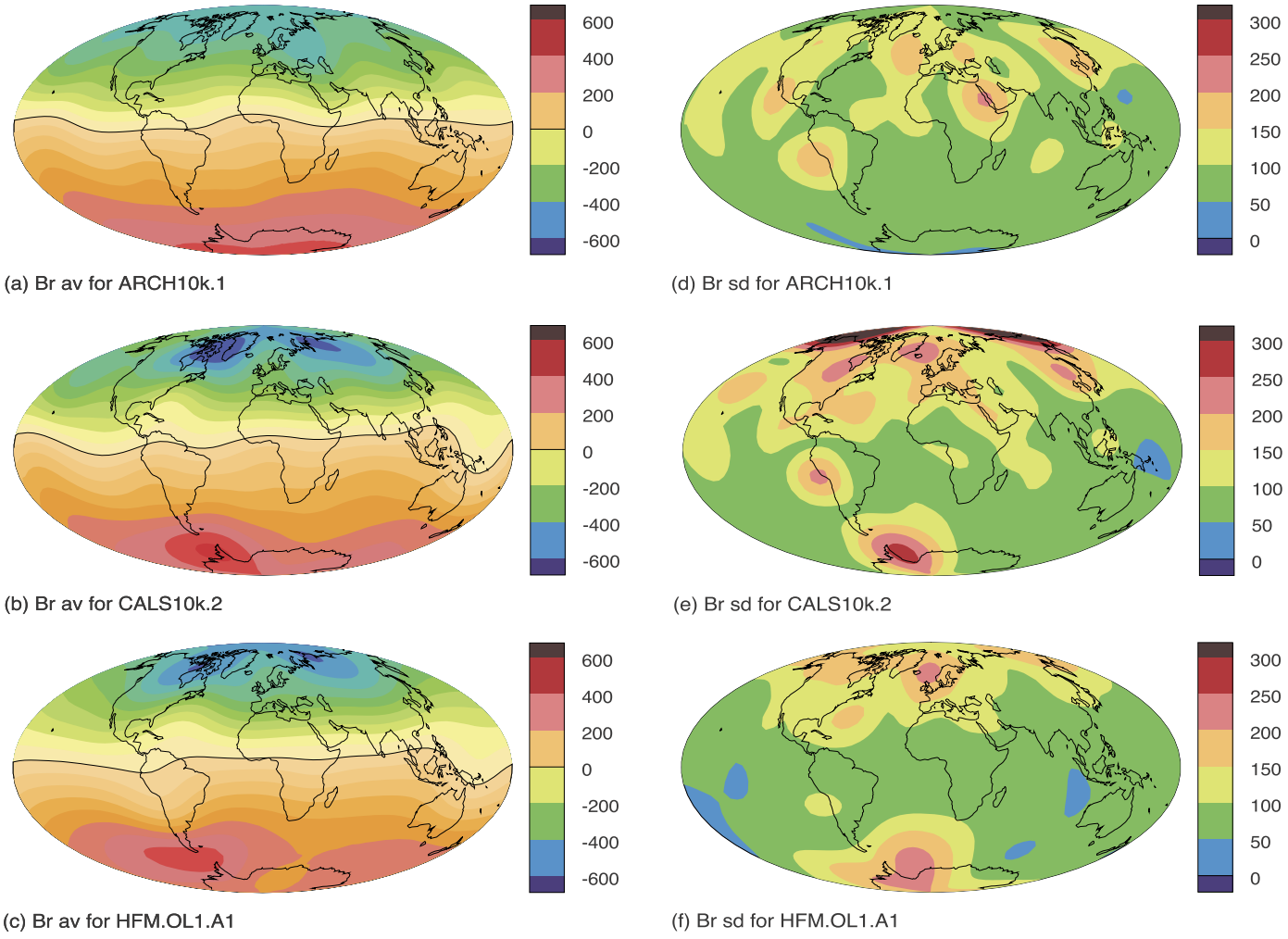

Fig. 7. Average B_r (μT) and its temporal standard deviation at CMB for preliminary calibration model *ARCH10k.1* (a, d) and final models *CALS10k.2* (b, e) and *HFM.OL1.A1* (c, f).

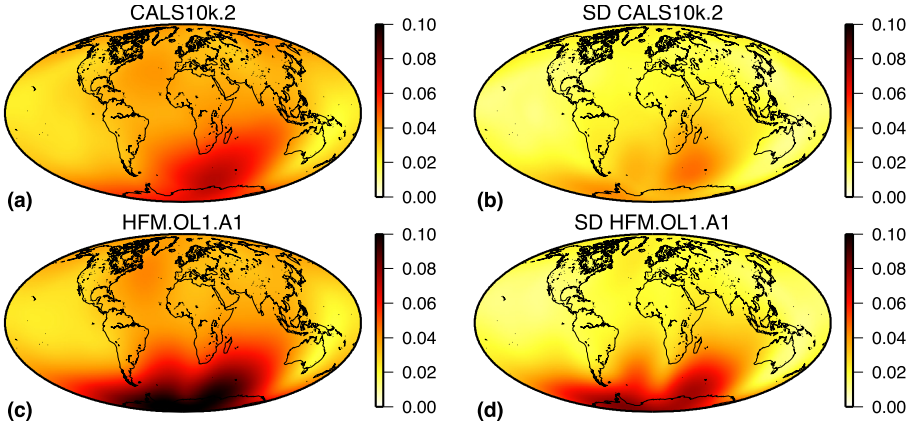

Fig. 8. (a), (c) PSV index, $\bar{P}_i$ for each of the time-averaged field models *HFM.OL1.A1* and *CALS10k.2*, and (b), (d) σ_{P_i}, its variability reflected in the temporal standard deviation. Note the concentration of activity in the southern hemisphere, and low values in equatorial and mid latitude Pacific regions. Excursional fields would be expected for $P_i > 0.5$.

Atlantic hemisphere than the Pacific region. The weakest signals in $\bar{P}_i$ correspond with regions of low Pacific secular variation in *gufm1*. These surface features generally support the views of B_r in Fig. 7, with the largest departures from an axial dipole structure evident in the southern hemisphere longitudinal variations. However, the contribution to P_i from directional variability tends to emphasize contrast in the southern hemisphere compared with B_r variations.

The greatest variability in P_i, represented by the activity index σ_{P_i}, the standard deviation in time samples throughout the models, also occurs at the highest southern latitudes and in the Southern Indian and Atlantic Oceans, supporting the idea of mobile, highly variable structures episodically contributing to a long term southern hemisphere gyre. In contrast the Northern Hemisphere index is somewhat subdued, and much less variable in time.

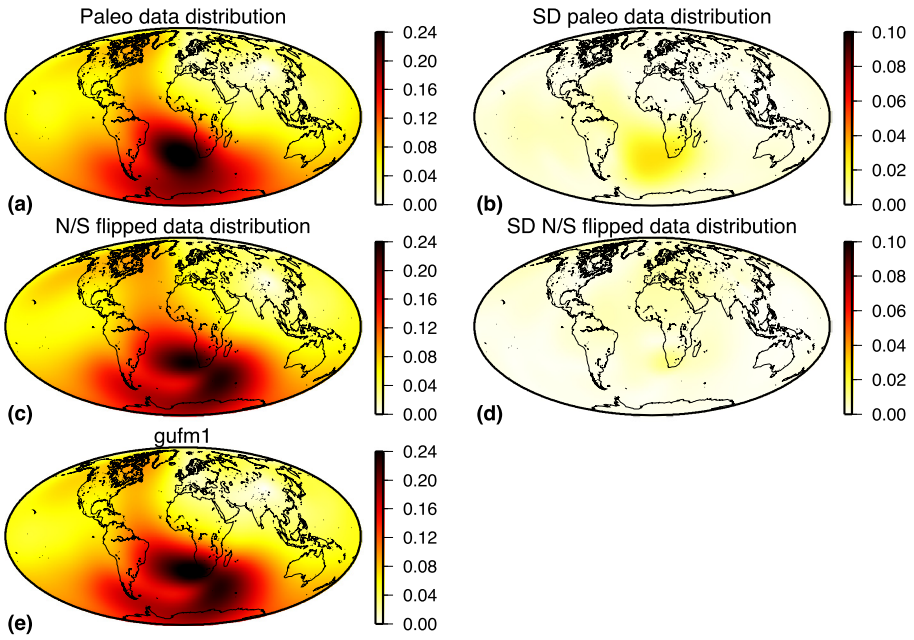

Fig. 9. Test of robustness for $\bar{P}_i$ evaluation using *gufm1* and temporally varying spatial and noise distribution of data. (a) P_i for the available temporally varying paleodata distribution; (b) σ_{P_i} for the same simulation as in (a); (c) P_i for data locations flipped between northern and southern hemisphere; (d) σ_{P_i} for the same simulation as in (c); (e) variability of $\bar{P}_i$ from *gufm1* in 1990 AD. Note that large scale variability in (e) is reproduced in the temporally average models (a, c) while the standard deviations due to noise and changing data locations in (b) and (d) are small in comparison with that due to the secular variation in *CALS10k.2* and *HFM.OL1.A1* (see Fig. 8).

Our results are inevitably influenced by the global distribution and quality of the data and by details of the modeling procedures. We tested the validity of our estimates for $\bar{P}_i$ and σ_{P_i} via simulations using the 1990 AD snapshot of *gufm1* and the actual temporally varying spatial distribution of data with realistic noise. Two test models were constructed and the results are illustrated in Fig. 9. In 9(a) and (c) 10 ky data samples were predicted from the constant 1990 *gufm1* model at the temporally changing data locations used for both *CALS10k.2* and *HFM.OL1.A1*. The structure of P_i is similar to that for *gufm1* in Fig. 9(e). The effect of changing data locations is barely visible in σ_{P_i} as shown in (b) and (d).

In our second test we flipped the data locations available in the northern and southern hemispheres to assess the effect of the sparse southern hemisphere distribution. Again the structure visible in P_i for the average model is similar to *gufm1* in 1990. The standard deviation remains well below the levels seen for the paleosecular variations in Fig. 8 for our new models.

These tests using a constant field for the entire 10 ky interval together with the available data distributions and assigned uncertainties indicate that these effects explain only a small fraction of the field variability found in *HFM.OL1.A1* and *CALS10k.2* (see Fig. 9). As more data come on line and provide better intensity calibrations and improved spatial coverage and temporal resolution, we can expect further refinements in field structure. Nevertheless, the large scale results presented here seem robust.

4. Discussion and conclusions

The average field strength in the southern hemisphere is weaker over the past 10 ky than in the north, as seen in Figs. 5(a) and 6(a), (c). Additionally, the Atlantic hemisphere has sustained consistently more active secular variation than the Pacific hemisphere (Figs. 7(e), (f) and 8(b), (d)) with a persistent focus of greater activity across the Indian and southern Atlantic Oceans.

The origin of these large scale differences in geomagnetic activity cannot yet be unequivocally identified. Steadily accumulated evidence from seismic observations and mineral physics experiments (Garnero et al., 2016) indicate that the lowermost mantle and core–mantle boundary are home to complex structure (with associated compositional and phase variations) which can inhibit or enhance heat flow from the core (Amit et al., 2015). Similarly, the inner core exhibits variable structure, with seismic velocities that are faster and more isotropic in the eastern than the western hemisphere (Deuss, 2014). Numerical dynamo simulations now routinely incorporate tomographic boundary conditions drawing on seismic velocity structures from the lowermost mantle and the top of the inner core, and have more recently evolved to include gravitational coupling between the inner core and mantle. Such simulations indicate that conditions at the core–mantle boundary and the inner-core boundary do influence outer core dynamics and produce visible signatures in long term averages of the geomagnetic field and core flow models. Recent studies (Aubert et al., 2013; Driscoll, 2015) suggest that large scale heterogeneities in conditions at the top or the bottom of the outer core may be visible in short term geomagnetic variations. However, the persistence of high regional PSV activity in our 10 kyr models cannot on their own resolve the question of how long a record is needed to detect the impact of mantle structure.

Large low seismic shear wave velocity provinces (LLSVPs) have been identified in extended regions of the lowermost mantle beneath Africa (Lekic et al., 2012) and the western Pacific. These are likely to provide geographically variable boundary conditions, that may well be different in each location, and are likely to have persisted for millions of years at least. A recent analysis (Ziegler and Constable, 2015) of geomagnetic paleointensity variations for the time interval 0–300 ka identifies differences in regional field variability associated with LLSVPs and those results are consistent with our work. The planetary scale gyre visible in the modern field may thus be a prominent feature over the longer term, with development of equatorial flux patches (and associated changes in dipole moment) produced as part of this dynamic. This idea is compatible with observations (Ziegler and Constable, 2015) that regional intensity minima associated with geomagnetic excursions are more pronounced and can appear first in the African LLSVP region, suggesting greater instability in the Atlantic hemisphere. This seems to require that the Pacific LLSVP has a different impact on the dy-

namics, perhaps reflecting a different balance between thermal and compositional structures in the super-plumes.

Do our results have any consequences for the question of dipole decay and potential incipient reversal? The current decay does not appear particularly unusual when viewed in the context of 0–10 ka variations, since the dipole moment has been unusually high for the past 3 ky. The recent decay may form part of a pattern of changes in dipole moment involving mixed large scale advection and diffusion mechanisms (Olson and Amit, 2006), with a significant contribution to dipole decay caused by advection of concentrations of normal flux towards the equator, along with growth of mid-latitude reverse flux patches in the southern hemisphere. Similarly, periods of dipole growth could be stimulated by poleward motion of normal polarity flux which, given the higher overall field strength, may occur preferentially in the north. More light could be cast on this topic by the acquisition of high quality 10 ky time series of paleosecular variation in and around Africa, the Indian Ocean and Australasia, potentially allowing the tracking of evolution of a series of equatorial flux patches over time. The acquisition of more detailed knowledge regarding the kinematics seems necessary before the deeper dynamical processes can be understood.

5. Author contributions

CC led the analysis and interpretation of output from models CALS10k.2 and HFM.OL1.A1 which were produced by MK and SP, respectively. All co-authors contributed to development of the manuscript with CC leading on the initial draft which was then read and modified by all co-authors.

Acknowledgements

We thank Christopher Davies for stimulating discussions, and Hagay Amit and an anonymous reviewer for detailed comments on our initial manuscript. CC and MK greatly appreciate support for their collaboration from the Alexander von Humboldt Foundation. CC and SP acknowledge support from NSF grant EAR-1246826, and MK from DFG KO 2870/5-1.

References

Amit, H., Aubert, J., Hulot, G., 2010. Stationary, oscillating or drifting mantle-driven geomagnetic flux patches? J. Geophys. Res. 115, B07108. http://dx.doi.org/10.1029/2009JB006542.

Amit, H., Deschamps, F., Choblet, G., 2015. Numerical dynamos with outer boundary heat flux inferred from probabilistic tomography—consequences for latitudinal distribution of magnetic flux. Geophys. J. Int. 203 (2), 840–855.

Aubert, J., Amit, H., Hulot, G., 2007. Detecting thermal boundary control in surface flows from numerical dynamos. Phys. Earth Planet. Inter. 160 (2), 143–156.

Aubert, J., Finlay, C.C., Fournier, A., 2013. Bottom-up control of geomagnetic secular variation by the Earth's inner core. Nature 502 (7470), 219–223.

Bloxham, J., Gubbins, D., 1985. The secular variation of Earth's magnetic field. Nature 317 (6040), 777–781.

Brown, M.C., Donadini, F., Korte, M., Nilsson, A., Korhonen, K., Lodge, A., Lengyel, S.N., Constable, C.G., 2015. GEOMAGIA50.v3: 1. General structure and modifications to the archeological and volcanic database. Earth Planets Space 67 (1), 83.

Constable, C., Korte, M., 2006. Is Earth's magnetic field reversing? Earth Planet. Sci. Lett. 246, 1–6.

Constable, C., Korte, M., 2015. Centennial- to millennial-scale geomagnetic field variations. In: Treatise on Geophysics. Elsevier, pp. 309–341.

Constable, C.G., 1988. Parameter-estimation in non-Gaussian noise. Geophys. J. (Oxf.) 94 (1), 131–142.

Davies, C.J., Gubbins, D., Willis, A.P., Jimack, P.K., 2008. Time-averaged paleomagnetic field and secular variation: predictions from dynamo solutions based on lower mantle seismic tomography. Phys. Earth Planet. Inter. 169 (1–4), 194–203.

De Santis, A., Qamili, E., 2015. Geosystemics: a systemic view of the Earth's magnetic field and the possibilities for an imminent geomagnetic transition. Pure Appl. Geophys. 172 (1), 75–89.

Deuss, A., 2014. Heterogeneity and anisotropy of Earth's inner core. Annu. Rev. Earth Planet. Sci. 42 (1), 103–126.

Driscoll, P.E., 2015. Testing the dynamic coupling of the core–mantle and inner core boundaries. J. Geophys. Res., Solid Earth 120. http://dx.doi.org/10.1002/2014JB011682.

Finlay, C.C., Aubert, J., Gillet, N., 2016. Gyre-driven decay of the Earth's magnetic dipole. Nat. Commun. 7, 10422.

Finlay, C.C., Jackson, A., Gillet, N., Olsen, N., 2012. Core surface magnetic field evolution 2000–2010. Geophys. J. Int. 189 (2), 761–781.

Garnero, E.J., McNamara, A.K., Shim, S.-H., 2016. Continent-sized anomalous zones with low seismic velocity at the base of Earth's mantle. Nat. Geosci. 9 (7), 481–489.

Gillet, N., Pais, M.A., Jault, D., 2009. Ensemble inversion of time-dependent core flow models. Geochem. Geophys. Geosyst. 10 (6), n/a–n/a.

Gubbins, D., 1975. Can the Earth's magnetic field be sustained by core oscillations? Geophys. Res. Lett. 2 (9), 409–412.

Gubbins, D., 1987. Mechanism for geomagnetic polarity reversals. Nature 326 (6109), 167–169.

Gubbins, D., Jones, A.L., Finlay, C.C., 2006. Fall in Earth's magnetic field is erratic. Science 312 (5775), 900–902.

Holme, R., Olsen, N., Bairstow, F.L., 2011. Mapping geomagnetic secular variation at the core–mantle boundary. Geophys. J. Int. 186 (2), 521–528.

Hulot, G., Eymin, C., Langlais, B., Mandéa, M., Olsen, N., 2002. Small-scale structure of the geodynamo inferred from Oersted and Magsat satellite data. Nature 416 (6881), 620–623.

Jackson, A., Jonkers, A.R.T., Walker, M.R., 2000. Four centuries of geomagnetic secular variation from historical records. Philos. Trans. R. Soc. Lond. A 358, 957–990.

Johnson, C.L., Constable, C.G., Tauxe, L., Barendregt, R., Brown, L.L., Coe, R.S., Layer, P., Mejia, V., Opdyke, N.D., Singer, B.S., Staudigel, H., Stone, D.B., 2008. Recent investigations of the 0–5 Ma geomagnetic field recorded by lava flows. Geochem. Geophys. Geosyst. 9 (4).

Korte, M., Constable, C., 2011. Improving geomagnetic field reconstructions for 0–3 ka. Phys. Earth Planet. Inter. 188 (3–4), 247–259.

Korte, M., Constable, C., Donadini, F., Holme, R., 2011. Reconstructing the Holocene geomagnetic field. Earth Planet. Sci. Lett. 312 (3–4), 497–505.

Korte, M., Donadini, F., Constable, C.G., 2009. Geomagnetic field for 0–3 ka: 2. A new series of time-varying global models. Geochem. Geophys. Geosyst. 10, Q06008. http://dx.doi.org/10.1029/2008GC002297.

Korte, M., Holme, R., 2010. On the persistence of geomagnetic flux lobes in global field models. Phys. Earth Planet. Inter. 182, 179–186.

Laj, C., Kissel, C., 2015. An impending geomagnetic transition? Hints from the past. Earth Sci. Front. 3. http://dx.doi.org/10.3389/feart.2015.00061.

Lekic, V., Cottaar, S., Dziewonski, A., Romanowicz, B., 2012. Cluster analysis of global lower mantle tomography: a new class of structure and implications for chemical heterogeneity. Earth Planet. Sci. Lett. 357–358, 68–77.

Merrill, R.T., McElhinny, M.W., McFadden, P.L., 1996. The Magnetic Field of the Earth: Paleomagnetism, the Core, and the Deep Mantle. Academic, San Diego.

Nilsson, A., Holme, R., Korte, M., Suttie, N., Hill, M., 2014. Reconstructing Holocene geomagnetic field variation: new methods, models and implications. Geophys. J. Int. 198, 229–248.

Olson, P., 2002. The disappearing dipole. Nature 416, 591–594.

Olson, P., Amit, H., 2006. Changes in Earth's dipole. Naturwissenschaften 93 (11), 519–542.

Olson, P., Driscoll, P., Amit, H., 2009. Dipole collapse and reversal precursors in a numerical dynamo. Phys. Earth Planet. Inter. 173 (1–2), 121–140.

Panovska, S., Constable, C.G., 2016. An activity index for geomagnetic paleosecular variation, excursions, and reversals. Geochem. Geophys. Geosyst. Revised for publication.

Panovska, S., Finlay, C.C., Donadini, F., Hirt, A.M., 2012. Spline analysis of Holocene sediment magnetic records: uncertainty estimates for field modeling. J. Geophys. Res. 117 (B2), B02101.

Panovska, S., Korte, M., Finlay, C.C., Constable, C.G., 2015. Limitations in paleomagnetic data and modelling techniques and their impact on Holocene geomagnetic field models. Geophys. J. Int. 202 (1), 402–418.

Tauxe, L., Shaar, R., Jonestrask, L., Swanson-Hysell, N.L., Minnett, R., Koppers, A.A.P., Constable, C.G., Jarboe, N., Gaastra, K., Fairchild, L., 2016. PmagPy: software package for paleomagnetic data analysis and a bridge to the Magnetics Information Consortium (MagIC) Database. Geochem. Geophys. Geosyst. 17 (6), 2450–2463.

Turner, G.M., Howarth, J.D., de Gelder, G.I.N.O., Fitzsimons, S.J., 2015. A new high-resolution record of Holocene geomagnetic secular variation from New Zealand. Earth Planet. Sci. Lett. 430, 296–307.

Wang, H., Kent, D.V., Rochette, P., 2015. Weaker axially dipolar time-averaged paleomagnetic field based on multidomain-corrected paleointensities from Galapagos lavas. Proc. Natl. Acad. Sci. 112 (49), 15036–15041.

Willis, A.P., Sreenivasan, B., Gubbins, D., 2007. Thermal core–mantle interaction: exploring regimes for 'locked' dynamo action. Phys. Earth Planet. Inter. 165 (1–2), 83–92.

Ziegler, L.B., Constable, C.G., 2015. Testing the geocentric axial dipole hypothesis using regional paleomagnetic intensity records from 0 to 300 ka. Earth Planet. Sci. Lett. 423, 48–56.